

We are IntechOpen, the world's leading publisher of Open Access books Built by scientists, for scientists

6,900

Open access books available

186,000

International authors and editors

200M

Downloads

Our authors are among the

154

Countries delivered to

TOP 1%

most cited scientists

12.2%

Contributors from top 500 universities



WEB OF SCIENCE™

Selection of our books indexed in the Book Citation Index
in Web of Science™ Core Collection (BKCI)

Interested in publishing with us?
Contact book.department@intechopen.com

Numbers displayed above are based on latest data collected.
For more information visit www.intechopen.com



Electromagnetic Wave Absorption Properties of Core-Shell Ni-Based Composites

Biao Zhao and Rui Zhang

Abstract

Currently, high efficiency electromagnetic wave absorption plays an important role to keep away from the detection of aircraft by radar and reduce information leakage in various electronic equipment. Among the candidates of electromagnetic absorbers, ferromagnetic Ni materials possess high saturation magnetization and high permeability at high frequency (1–18 GHz), which is widely used to prepare thinner absorbing materials along with strong electromagnetic absorption properties. However, the metallic materials usually have relatively high electrical conductivity, and their permeability decreases rapidly at high frequency thanks to the eddy current losses, which is generally named as skin-depth effect. To address this issue, one effective way is to design core-shell structured Ni based composites combining magnetic cores with dielectric shells. This chapter focuses on the state-of-the-art of the microwave absorption properties of Ni-based core-shell composites, and the related electromagnetic attenuation theory about how to enhance absorption properties is also discussed in detail.

Keywords: ferromagnetic Ni, core-shell structure, dielectric loss, magnetic loss, impedance match

1. Introduction

The discovery of electromagnetic (EM) waves boosted the development of transmission technology. It is well accepted that the various electromagnetic waves are widely applied in numerous areas and make our daily life convenient [1]. Extensive electronics devices, such as mobile phones, WiFi, Near Field Communication (NFC), and wireless charging, are developing and play an important role in modern life [2, 3]. With the extensive practical applications of electronic devices and densely packed systems, electromagnetic interference (EMI) becomes a more and more serious problem, which would lead to pernicious impacts on equipment performance, human health, as well as surrounding environment [4]. Furthermore, our individual mini device produces unwanted EM waves, which would influence other nearby devices [5]. Moreover, the global need for some EM waves, such as for military radar stealth, is also boosting, which produces plentiful concerns for human health. Therefore, the protection of electromagnetic radiation has been widely concerned by the whole society. Recently, development of high

performance microwave absorbing materials (MAMs) have attracted great interests to eliminate the electromagnetic pollution [6, 7].

Recently, considerable research attention has been focused on core-shell structure for innovative electromagnetic absorption due to the potential to combine the individual properties of each component or achieve enhanced performances through cooperation between the components [8–10]. Liu and co-workers have fabricated core-shell structured $\text{Fe}_3\text{O}_4@\text{TiO}_2$ with Fe_3O_4 as cores and hierarchical TiO_2 as shells and the $\text{Fe}_3\text{O}_4@\text{TiO}_2$ core-shell composites displayed the enhanced microwave absorption properties than pure Fe_3O_4 [11]. Chen and co-workers have successfully synthesized core/shell $\text{Fe}_3\text{O}_4/\text{TiO}_2$ composite nanotubes with superior microwave attenuation properties [12]. Combining Fe_3O_4 and TiO_2 can take advantage of both the unique magnetic properties of Fe_3O_4 and strong dielectric characteristics of TiO_2 as well as core-shell structure, and therefore offer an avenue to achieve excellent microwave-absorption performance. In this kind of core/shell configurations, the magnetic materials regarding as cores, which could improve the permeability of the composites, is conducive to the enhancement of the magnetic loss. The dielectric materials considering as shells, which are supposed to play the roles not only as a center of polarization but also as an insulating medium between the magnetic particles, lead to the increased dielectric loss and good impedance match. The high-efficiency microwave absorption properties resulted from the enhanced magnetic loss, dielectric loss, reduced eddy current loss and impedance match [8]. Thus, the traditional microwave absorbing materials holding a core-shell structure may improve their microwave absorption capabilities.

It is well known Ni is regarded as a typical magnetic metal material, which are supposed to have numerous applications in many fields such as magnetic recording devices, clinical medicine, catalysis and so on [13, 14]. It is worth pointing that Ni was also proved to be as a competitive candidate for high-efficiency electromagnetic absorption materials to address the electromagnetic interference and pollution problems because Ni can provide more beneficial features, such as high saturation magnetization, distinguishable permeability, and compatible dielectric loss ability in the gigahertz range when compared with those nonmagnetic EM absorption materials. However, single-component electromagnetic absorption materials easily suffer from mismatched characteristic impedance and poor microwave absorption performance. Moreover, Ni would generate eddy current induced by microwave in GHz range because of high conductivity. The eddy current effect may cause impedance mismatching between the absorbing materials and air space, which would make microwave reflection rather than absorption. This issue is a challenge to handle for scientists. Thus, for the sake of getting superior microwave absorption ability, a promising pathway is to compound the Ni products with an inorganic or nonmagnetic constituent to produce a core@shell configuration. Numerous literatures have been carried out to cover the magnetic Ni with inorganic or nonmagnetic shells. For example, Ni/ SnO_2 core-shell composite [15], carbon-coated Ni [16], Ni/ ZnO [17], Al/ AlO_x -coated Ni [18], Ni@ Ni_2O_3 core-shell particles [19], Ni/polyaniline [20], and CuO/ Cu_2O -coated Ni [21] show the better microwave absorption performance than the pure core or shell materials. Thus, the EM wave absorption abilities of Ni particles can be obviously enhanced after coating inorganic and nonmagnetic shells.

Herein, we report the microwave absorption properties of core-shell structured Ni based composites and discuss how does core-shell ameliorate the electromagnetic wave absorption properties and also investigate the related electromagnetic attenuation theory in detail.

2. Core-shell Ni@oxide composite as microwave absorbers

2.1 Core-shell Ni@ZnO composites as microwave absorbers

For the ZnO nanostructural materials, due to the features of lightweight semi-conductive properties and its easily mass synthesis, they are expected to be the potential applications in EM wave absorbing materials [22]. Therefore, when the Ni particles were covered by ZnO shell, the electromagnetic properties of Ni would be boosted, correspondingly. Moreover, it is well accepted that the EM absorption properties are closely related with their morphologies. Herein, the various morphologies of Ni/ZnO composites were synthesized by control of the amounts of $\text{NH}_3\cdot\text{H}_2\text{O}$, and the microwave absorption properties of these Ni/ZnO composites have been investigated based on the complex permittivity and permeability.

2.1.1 Preparation of core-shell Ni@ZnO composites

Ni microspheres were prepared based on our previous publication [15]. Ni/ZnO composites were synthesized through a facile hydrothermal method [23]. Typically, 0.05 g of the as-obtained Ni microspheres was distributed in 60 mL distilled water. Then 0.45 g of $\text{Zn}(\text{CH}_3\text{COO})_2\cdot 2\text{H}_2\text{O}$ and a certain amounts of ammonia solution were added into the mixture solution. The mixture was transferred into a Teflon-lined stainless steel autoclave, and maintained at 120°C for 15 h. The precipitates were collected by centrifugation, washed several times with distilled water and absolute ethanol, respectively. For the convenience of discussion, the Ni/ZnO prepared at 1 mL $\text{NH}_3\cdot\text{H}_2\text{O}$, 2 mL $\text{NH}_3\cdot\text{H}_2\text{O}$ and 3 mL $\text{NH}_3\cdot\text{H}_2\text{O}$ were denoted as SA, SB and SC, respectively.

Figure 1a displays the representative FESEM image of the Ni particles, which possesses uniformly spherical shape and the diameter is about 1.0–1.2 μm . The SEM images of the Ni/ZnO obtained at different contents of $\text{NH}_3\cdot\text{H}_2\text{O}$ are displayed in **Figure 1b–d**. **Figure 1b** exhibits that the as-prepared Ni/ZnO product is composed of plentiful ZnO polyhedrons with the diameter of 0.2–0.5 μm covered on the surface of Ni particles to generate special core-shell structure if small amount of $\text{NH}_3\cdot\text{H}_2\text{O}$ (1 mL) was added. If the content of $\text{NH}_3\cdot\text{H}_2\text{O}$ is lifted to 2.0 mL, the football-like Ni/ZnO samples with the size of 4–5 μm could be observed (**Figure 1c**). One can infer that the thickness of ZnO polyhedron is about 2–3 μm , which is larger than that of Ni microsphere. Therefore, the Ni microspheres are completely coated by ZnO, thus, we could not see the existence of individual Ni microspheres. When the content of $\text{NH}_3\cdot\text{H}_2\text{O}$ is further improved to 3 mL, ZnO rods and Ni microsphere coexist in the final products (**Figure 1d**), separately. These results indicate that the morphology of Ni/ZnO composite can be effectively adjusted by controlling the $\text{NH}_3\cdot\text{H}_2\text{O}$ content.

Figure 2 depicts the schematic diagram of the generation for various shapes of Ni/ZnO composite. First, the distributed Ni microspheres are fabricated through a chemical reduction method. Following, the different shapes of Ni/ZnO composites are fabricated by the addition of various $\text{NH}_3\cdot\text{H}_2\text{O}$ contents. The ZnO nuclei is prone to plant along special crystal planes and finally generate polyhedron-like or rod-like ZnO products. It is accepted that ZnO is a polar crystal with a polar c-axis ([0001] direction) [24]. In the solution system, the $\text{NH}_3\cdot\text{H}_2\text{O}$ consists of the positive hydrophilic group (NH_4^+) and negative hydrophobic group (OH^-). The positive hydrophilic groups would link with the basic cells of crystalline growth $[\text{Zn}(\text{OH})_4]^{2-}$ easily by Coulomb force, which means that the positive hydrophilic groups turn into the carriers of $[\text{Zn}(\text{OH})_4]^{2-}$; on the other hand, due to existence

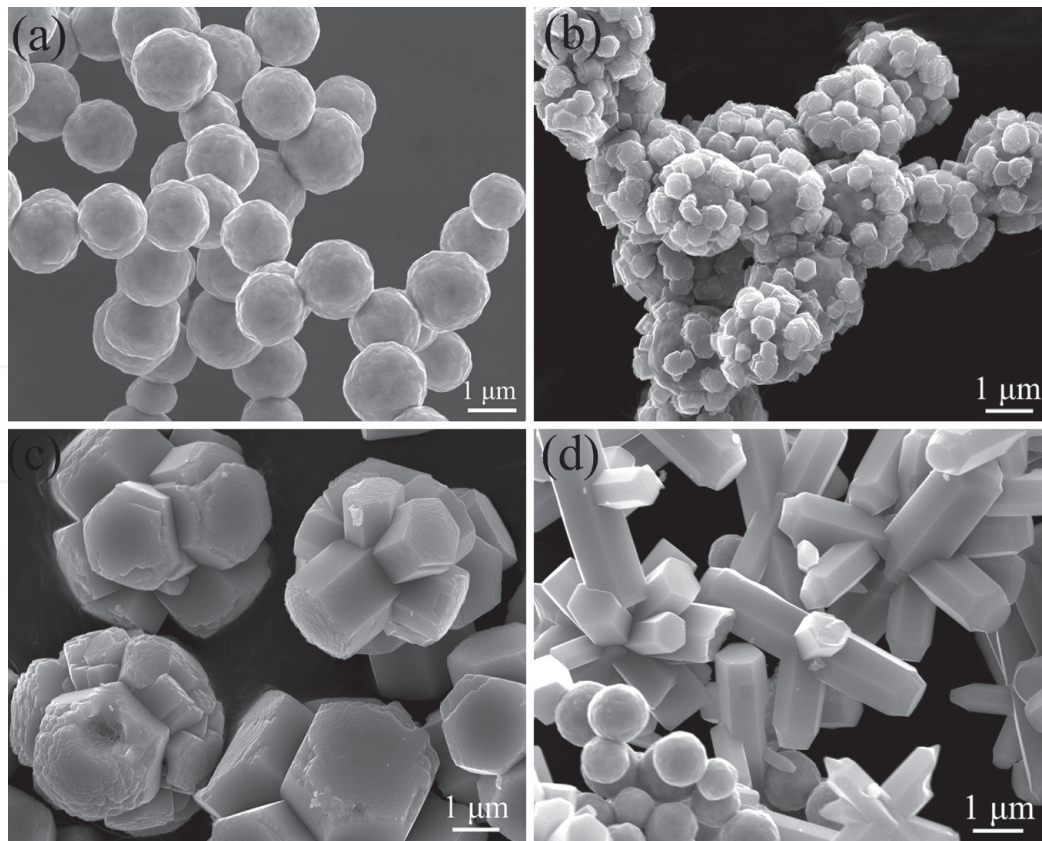


Figure 1. (a) SEM image of pure Ni microspheres and (b–d) SEM images of as-prepared Ni/ZnO samples prepared at various concentration of $\text{NH}_3\cdot\text{H}_2\text{O}$: (b) 1 mL, (c) 2 mL, and (d) 3 mL [23] (permission from Elsevier).

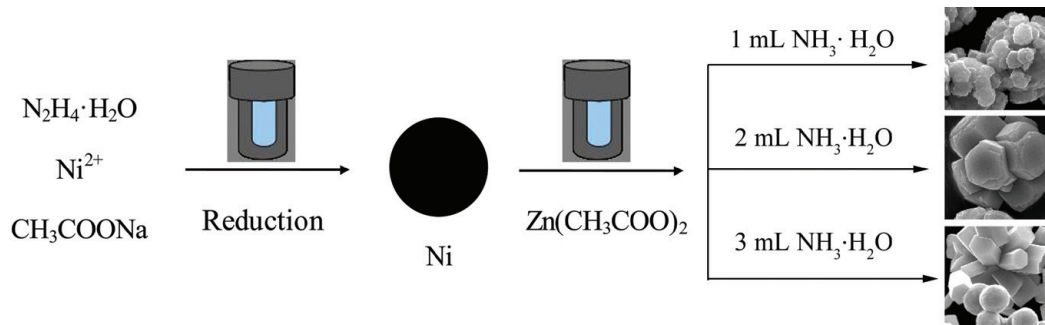


Figure 2. Schematic illustration of formation of various morphologies of Ni/ZnO composites [23] (permission from Elsevier).

of van der Waals force, the connection between the negative hydrophobic groups and the non-polar lateral surfaces of ZnO would take place, indicating that the occurrence of hydrophobic films thanks to the negative hydrophobic groups on the non-polar lateral surfaces [25]. The basic cells of growing $[\text{Zn}(\text{OH})_4]^{2-}$ attracted by the positive hydrophilic groups would move to the polar axial surface (0001) easily to integrate together and remain at the suitable lattice locations but difficultly reach the non-polar lateral remains due to the presence of the hydrophobic films. It indicates that the positive polar surface (0001) grows quicker than that of non-polar lateral surfaces in a fixed content of $\text{NH}_3\cdot\text{H}_2\text{O}$. As a result, more OH^- ions assimilate and hamper the growth on the positively charged (0001) surface, forcing a shape transition [26]. At the high content of $\text{NH}_3\cdot\text{H}_2\text{O}$, long ZnO nanorods could be produced because of the fast growth rate along the [0001] direction [27].

2.1.2 EM properties of core-shell Ni@ZnO composites

To reveal the electromagnetic wave absorption properties of SA, SB and SC paraffin composites, the reflection loss (RL) values of the Ni/ZnO samples are calculated based on following equations [28]:

$$RL = 20 \log_{10} |(Z_{in} - Z_0) / (Z_{in} + Z_0)| \quad (1)$$

$$Z_{in} = Z_0 \sqrt{\frac{\mu_r}{\epsilon_r}} \tanh \left(j \frac{2\pi f d \sqrt{\mu_r \epsilon_r}}{c} \right) \quad (2)$$

Herein Z_0 is the impedance of free space, Z_{in} is the input impedance of the material, f is the frequency of the microwave, c is the velocity of microwave in free space, μ_r and ϵ_r are, respectively, the relative complex permeability and permittivity, and d is the thickness of the absorber. The RL values of the three samples with a thickness of 2.0 mm are displayed in **Figure 3a**. The SA sample holds the outstanding EM wave absorption performances. A strong peak (-48.6 dB) could be seen at 13.4 GHz. The RL less than -10 dB (90% absorption) reaches 6.0 GHz (10.5–16.5 GHz). Furthermore, the RL less than -20 dB (99% microwave dissipation) is also obtained in the range of 11.5–14.2 GHz. But, for the SB and SC samples, they present inferior microwave dissipation capabilities. **Figure 3b** depicts the simulated RL of SA paraffin-composite with various thicknesses in the frequency of 1–18 GHz. Clearly, one can notice that the optimal RL shifts into lower frequency range along with an increased thickness, indicating that we could adjust the absorption bandwidth by tuning absorber thickness. From above analysis, one can note that the minimal RL of -48.6 dB could be observed at 13.4 GHz with a layer thickness of 2.0 mm. The effective absorption (below -10 dB) bandwidth could be monitored in the frequency of 9.0–18.0 GHz by control of the absorber thickness between 1.5 mm and 2.5 mm. Furthermore, the frequency with RL below -20 dB could be observed at 11.1–16.2 GHz with thickness of 1.8–2.2 mm. For the SA sample, the enhanced microwave absorption properties are stemmed from the good impedance match, synergistic effect between dielectric loss and magnetic loss, and special core-shell microstructures, which could induce the interference of microwave multiple reflection [29]. In addition, the compact polyhedron ZnO coating brings the metal/dielectric interfaces, in which the interface polarization boosts the microwave dissipation. For the football-like Ni/ZnO (SB), the size of ZnO is so big that the Ni microspheres could not interact with incident microwave, which

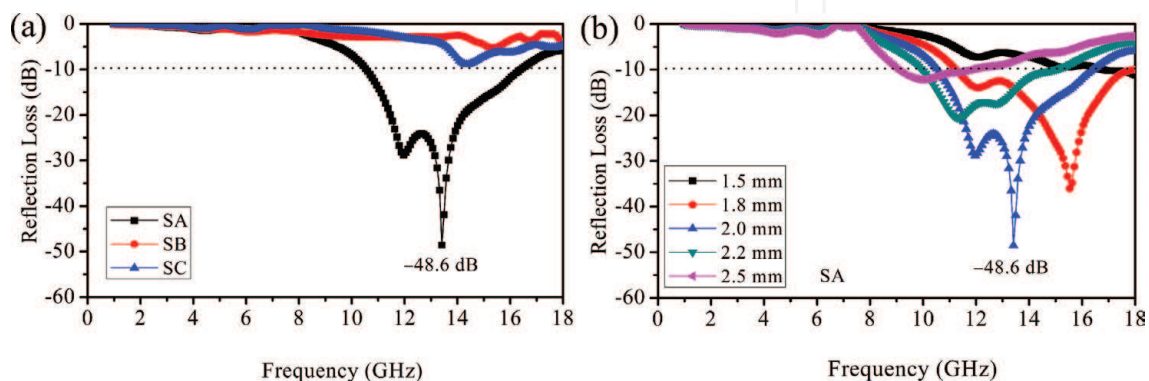


Figure 3. (a) Frequency dependences of RL with the thickness of 2.0 mm for the three samples SA, SB, SC; (b) RL of Ni/ZnO (SA) paraffin composite of varying thicknesses [23] (permission from Elsevier).

gives rise to the mismatch between the magnetic loss and dielectric loss, leading to inferior microwave absorption. For the SC, due to the presence of uncoated Ni, these uncoated Ni microspheres play a negative in the wave-absorption of materials thanks to the occurrence of a significant skin effect when its surface is irradiated by microwaves [30].

On the basis of transmission line theory, the suitable microwave absorption properties are determined by two key factors. One factor is the impedance match, which need the complex permittivity is close to the complex permeability, and the other one is the EM attenuation ability, which dissipates the microwave energy through dielectric loss or magnetic loss. The EM attenuation was determined by the attenuation constant α , which can be expressed as [31, 32]:

$$\alpha = \frac{\sqrt{2} \pi f}{c} \times \sqrt{(\mu'' \varepsilon'' - \mu' \varepsilon') + \sqrt{(\mu'' \varepsilon'' - \mu' \varepsilon')^2 + (\mu' \varepsilon'' + \mu'' \varepsilon')^2}} \quad (3)$$

where f is the frequency of the microwave and c is the velocity of light. **Figure 4** displays the frequency dependence of the attenuation constant. The SA possesses the biggest α in all measured frequency ranges, meaning the outstanding attenuation. Moreover, based on the above equation, one can notice that the attenuation constant is closely related to the values of ε'' and μ'' . The highest ε'' and μ'' values are the responsible for the highest α in Ni@ZnO (SA) core/shell structures, which is related to interface polarization and relaxation. As a result, the enhancement of the microwave absorption properties for the dielectric coating originates from the improvement of dielectric loss and magnetic loss.

2.2 Core-shell Ni@CuO composites as microwave absorbers

Nowadays, CuO is well accepted as an important p-type semiconductor, which holds the unique features of narrow band gap ($E_g = 1.2$ eV), and has captured more and more interests. This material has proved to exhibit widespread potential applications in optical switches, anode materials, field emitters, catalyst, gas sensors, photoelectrode and high-temperature micro-conductors [33, 34]. Recently, CuO has been realized as an efficient material for the preparation of microwave absorbing materials [21, 35, 36]. Herein, we fabricated the core-shell structural composites with Ni cores and rice-like CuO shells via a facile method. The microwave absorption properties of Ni, CuO and Ni/CuO composites are studied in term of complex

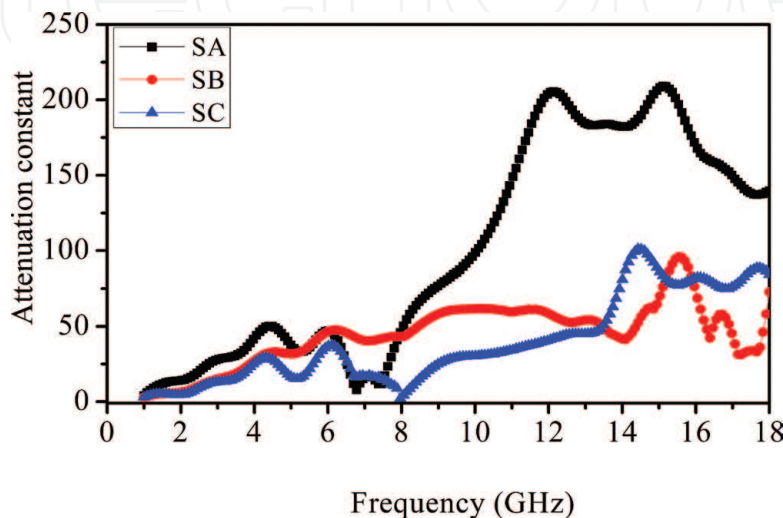


Figure 4. Attenuation constant of Ni/ZnO samples-paraffin composites versus frequency [23] (permission from Elsevier).

permittivity and permeability. In comparison with pristine Ni and CuO, rice-like CuO-coated Ni composites displayed the enhanced microwave absorption properties. Furthermore, we also studied the effects of CuO amounts on microstructures and microwave absorption properties of Ni/CuO composites in detail.

2.2.1 Preparation of core-shell Ni@CuO composites

The Ni microspheres were prepared by a solvothermal method, which was described in our pervious literature [15]. Synthesis of CuO nanoflakes: $\text{CuCl}_2 \cdot 2\text{H}_2\text{O}$ (0.36 g) was dissolved in a mixture of distilled water (60 mL) and ammonia (2 mL) under continuously stirring (30 min); The final mixture was transferred into a Teflon-lined autoclave and heated hydrothermally at 150°C for 15 h.

Synthesis of CuO rice-coated Ni core/shell composites [37]: the as-prepared Ni microspheres (0.05 g) and $\text{CuCl}_2 \cdot 2\text{H}_2\text{O}$ (0.36 g) were both added in distilled water (60 mL). Then, the ammonia (2 mL) was introduced into the mixture. Finally, the prepared mixture was moved into a Teflon-lined autoclave. The Teflon-lined autoclave was sealed and kept at 150°C for 15 h. The Ni/CuO composites prepared at 0.18 g $\text{CuCl}_2 \cdot 2\text{H}_2\text{O}$, 0.36 g $\text{CuCl}_2 \cdot 2\text{H}_2\text{O}$ and 0.54 g $\text{CuCl}_2 \cdot 2\text{H}_2\text{O}$ were denoted as S-1, S-2 and S-2, respectively.

Figure 5c, d exhibits FESEM micrographs of Ni@CuO composites with different magnification after hydrothermal treatment at 150°C for 15 h. It can be observed that the products are composed of CuO rices-coated smooth Ni microspheres heterostructures with the diameter of 1.0–1.2 μm . One can notice that rice-like CuO/Ni composites hold rough surfaces, which results from compactly aggregated panicle-shape CuO nanostructures. In order to get more information about microstructure of Ni/CuO composite, TEM and HR-TEM images of Ni/CuO composites are carried out. The core-shell structure of Ni/CuO composite can be

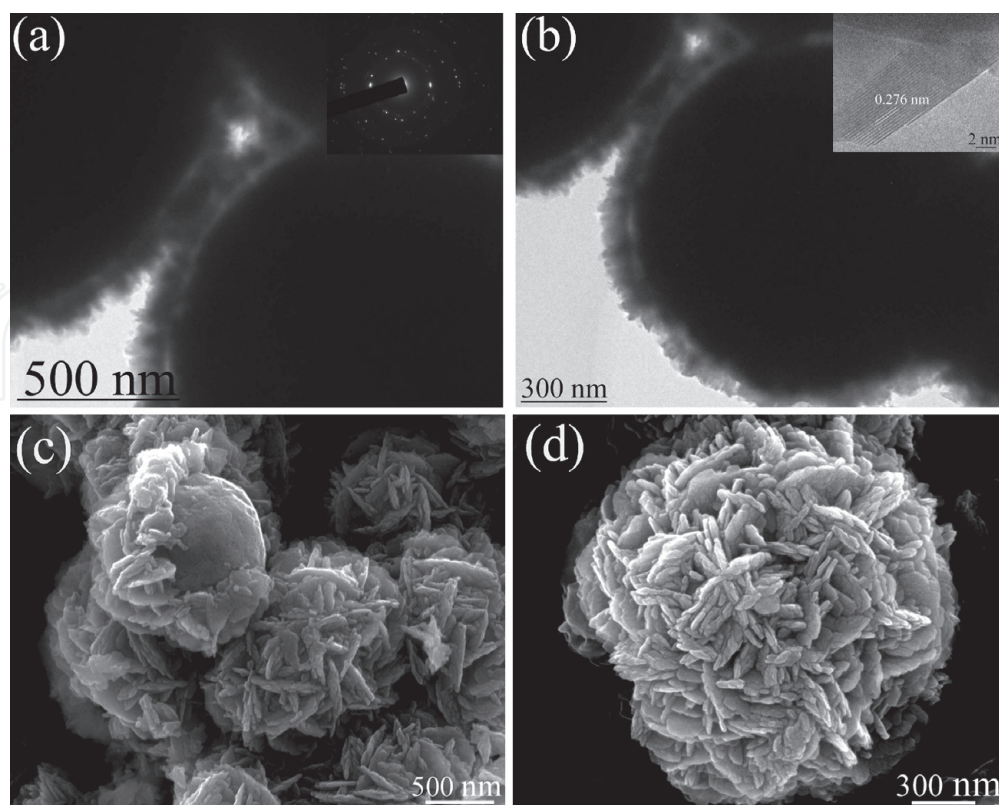


Figure 5. Typical TEM and HRTEM images of the as-prepared Ni/CuO structures: (a) low magnification, inset of (a) shows the SAED pattern; (b) high magnification; inset of (b) shows the HRTEM. (c, d) FESEM images of the Ni microsphere-CuO rice core-shell structures [37] (permission from RSC).

clearly observed from **Figure 5a, b**. The inset SAED pattern of the CuO particles indicated that CuO particles are polycrystalline (**Figure 5a**). The HRTEM image (inset of **Figure 5b**) displays that the lattice spacing is 0.276 nm, which is in good agreement with the (110) lattice spacing of CuO. Based on the SEM and TEM results, it can be concluded that the CuO is deposited on the surface of Ni, the core-shell composites are obtained under this procedure.

Figure 6 exhibits the morphologies of the obtained products with different molar ratio of the $\text{CuCl}_2 \cdot 2\text{H}_2\text{O}$ to Ni microspheres. Noticeably, the surfaces of all samples turns coarser in comparison with the pure Ni microspheres, which indicates the successful coating of the CuO nanoparticles on the pristine Ni surfaces. Furthermore, the shape and coverage density of CuO materials could be controlled by tuning the content of precursor (Cu^{2+}). When the molar ratio of the $\text{CuCl}_2 \cdot 2\text{H}_2\text{O}$ to Ni microspheres in the precursor solution is 1: 0.85 (S-1), one can find (**Figure 6a, b**) that the Ni microspheres are coated by a large number of CuO nanorices. But, due to the low content of precursor (Cu^{2+}), we just could obtain thin CuO shell. If the

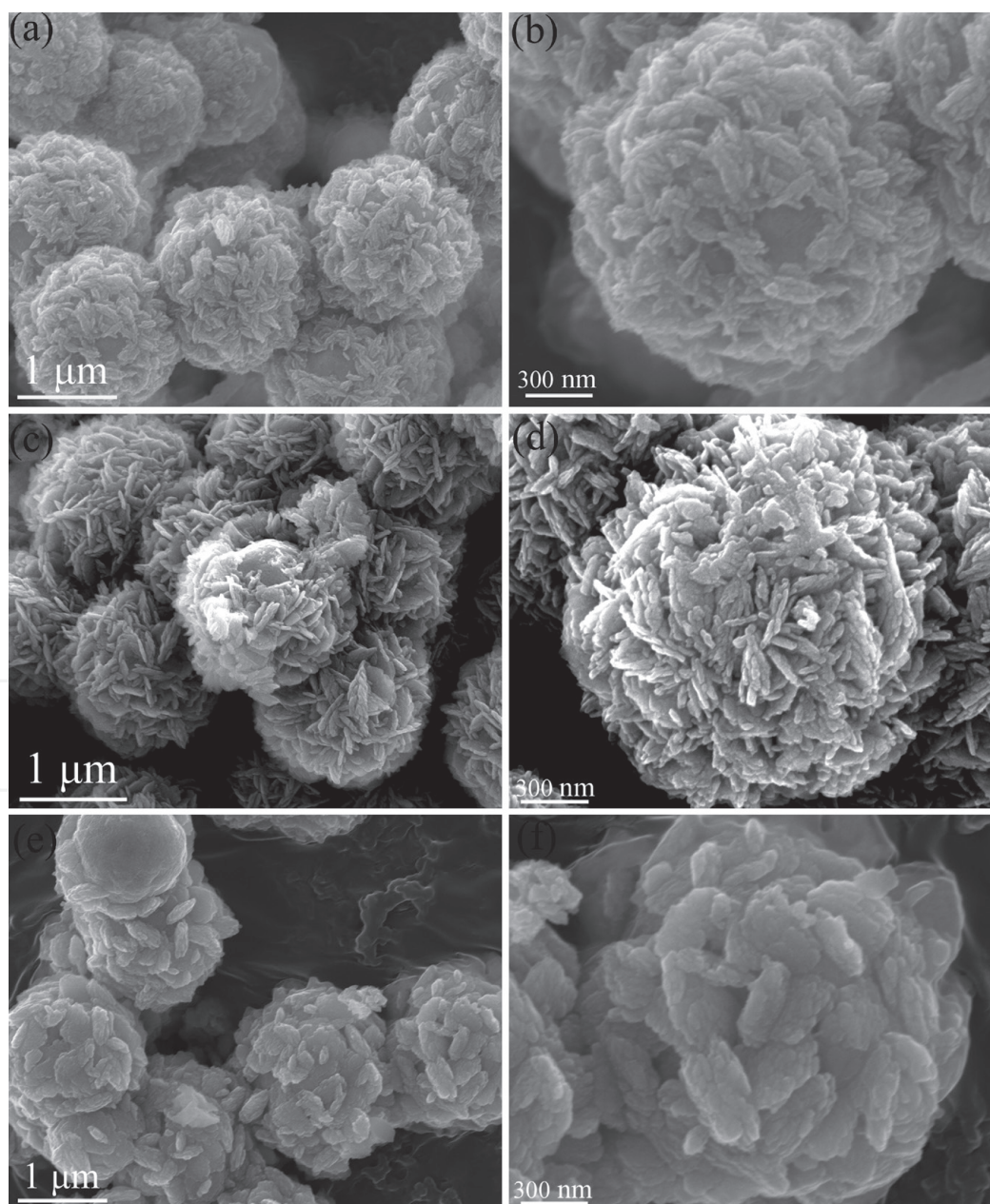


Figure 6. FESEM images of hierarchical Ni/CuO core-shell heterostructures with different molar ratio: (a, b) S-1; (c, d) S-2; and (e, f) S-3 [37] (permission from RSC).

molar ratio of precursor is enhanced to 2: 0.85 (S-2), one can see that the aggregation occurs and CuO nanorices are compactly covered on the smooth surfaces of Ni microspheres to produce coarser thick CuO shells (Figure 6c, d). If the molar ratio is improved continuously to 3:0.85 (S-3), a thick layer of compact CuO nanoflakes coated on Ni microspheres could be observed (Figure 6e, f). Based on above results, the microstructures and coverage density of CuO shells can be effectively monitored by selecting a suitable content of Cu^{2+} .

2.2.2 EM properties of core-shell Ni@CuO composites

To compare and assess the EM wave absorption properties of Ni, Ni/CuO core-shell composites, and CuO nanoflakes, the paraffin (30 wt%, which is transparent to microwave) are mixed with as-obtained products, and pressed into a ring shape with an outer diameter of 7.00 mm and an inner diameter of 3.04 mm. The microwave absorption abilities of these as-fabricated products could be evaluated by the RL values, which could be simulated on the basis of the complex permeability and permittivity with the measured frequency and given layer thickness [38, 39]. As presented in Figure 7a, the three Ni/CuO composites show the superior microwave-absorption properties to those of the pure Ni microspheres and the CuO nanoflakes. Taking an example, when the thickness is 2 mm, the S-1 sample exhibits the enhanced EM-wave absorption with the minimal RL value of -15.6 dB at 11.9 GHz among the five samples. From Eqs. (1) and (2), one can find that the thickness of the absorber is one important factor, which would affect the position of minimal RL value and the absorption bandwidth. Therefore, the RL values of Ni/CuO samples with different thicknesses are also calculated. Compared with S-2 (Figure 7c) and S-3 (Figure 7d) samples, the S-1 (Figure 7b) displays the outstanding microwave absorption performances. The lowest RL of the S-1 sample is -62.2 dB at 13.8 GHz with the only thickness of 1.7 mm. The effective absorption (below -10 dB) bandwidth can be tuned between 6.4 GHz and 18.0 GHz by adjusting thickness in 1.3–3.0 mm.

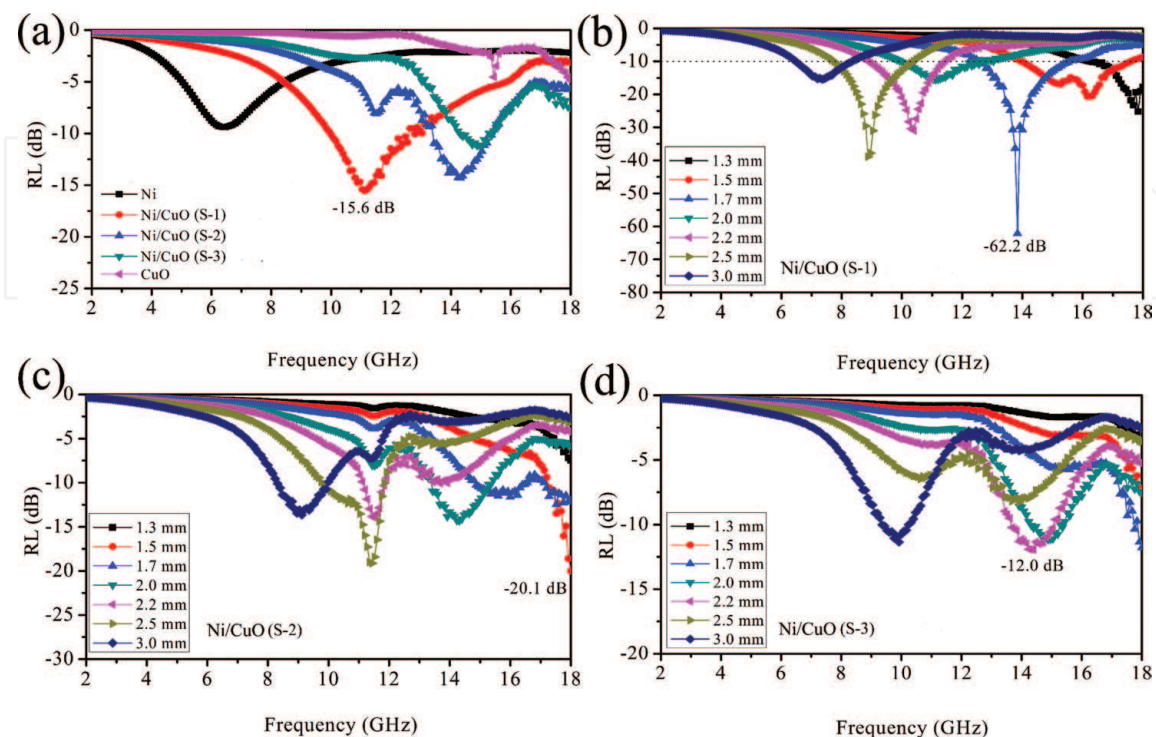


Figure 7. (a) Comparison of RL of the five as-obtained samples with a thickness of 2.0 mm. The RL values of (b) S-1, (c) S-2, and (d) S-3 samples with various thicknesses [37] (permission from RSC).

Notably, the optimal RL peaks gradually shift toward lower frequencies with an increased absorber thickness, which can be described by quarter-wavelength cancelation model that the incident and reflected waves in the absorber are out of phase 180° and causing the reflected waves in the air-absorber interface are totally cancelled [40]. The enhanced microwave absorption property of core-shell Ni/CuO composites can be obtained by tuning the content of CuO. The rice-like CuO shell is expected to be helpful for the dissipation proprieties of the core/shell composites. The CuO shells are covered on the surface of Ni microspheres to produce the special core-shell structure, which brings metal-dielectric hetero-interfaces to cause interfacial polarization. It is supposed that the interfacial polarization taken place in heterostructures consisting of at least two constituents [17, 41, 42]. This type of polarization occurring at the interfaces results from the movement of charge carriers between different compositions, which accumulate the moving charge at these interfaces. When irradiated by alternating EM fields, the accumulated charge would redistribute periodically between Ni cores and CuO shells, which are favorable for the microwave dissipation. However, for the S-2 and S-3 samples, thanks to the high content of CuO, we cannot observe the synergistic effect between Ni cores and CuO shells, which gives rise to inferior microwave absorption.

3. Core-shell Ni@non-oxide composite as microwave absorbers

3.1 Ni@ZnS composites as microwave absorbers

It is well known that ZnS, a wide band-gap semiconductor with the band-gap energy (E_g) of 3.6 eV, has been widely applied in displays, sensors, and lasers for many years [43, 44]. As far as I am concerning, the publications about the microwave absorption properties of ZnS and core/shell structured Ni/ZnS are not reported. Herein, we synthesized the core-shell structured composites with Ni cores and ZnS nanowall shells through a facile method. The microwave absorption properties of Ni, ZnS and Ni@ZnS composites are detailedly investigated in the frequency of 2–18 GHz.

3.1.1 Preparation of core-shell Ni@ZnS composites

ZnS nanowall-coated Ni composites were fabricated via a two-stage method [45]. First, Ni microspheres were synthesized based on our previous paper [15]. Second, Ni microspheres are coated by ZnS nanowalls to generate the core-shell structural composites. In the modified procedure, the as-obtained Ni microspheres (0.05 g) and $\text{Zn}(\text{CH}_3\text{COO})_2 \cdot 2\text{H}_2\text{O}$ (0.45 g) were added in a mixture solution of ethanol (30 mL) and distilled water (30 mL). Then, $\text{Na}_2\text{S} \cdot 9\text{H}_2\text{O}$ (0.50 g) and ammonia solution (4 mL) were added into the mixture solution with intensely stirring for 20 min. Finally, the mixture was moved into a Teflon-lined stainless steel autoclave, and kept at 100°C for 15 h. In order to study the effect of core-shell structure on the microwave absorption properties of the Ni/ZnS composite, the pure ZnS particles were also prepared according to the above procedure without addition of Ni microspheres.

Inset of **Figure 8a** presents the XRD profiles of Ni microspheres, ZnS particles and Ni@ZnS composites. For the Ni microspheres, all the diffraction peaks can be well indexed to the face-centered cubic (fcc) structure of nickel (JCPDS No. 04-0850). For the ZnS particles, all diffraction peaks can be indexed to a typical zinc blende structured ZnS, which is consistent with the standard value for bulk ZnS (JCPDS Card No. 05-0566). The crystal structure of core/shell structured Ni/ZnS

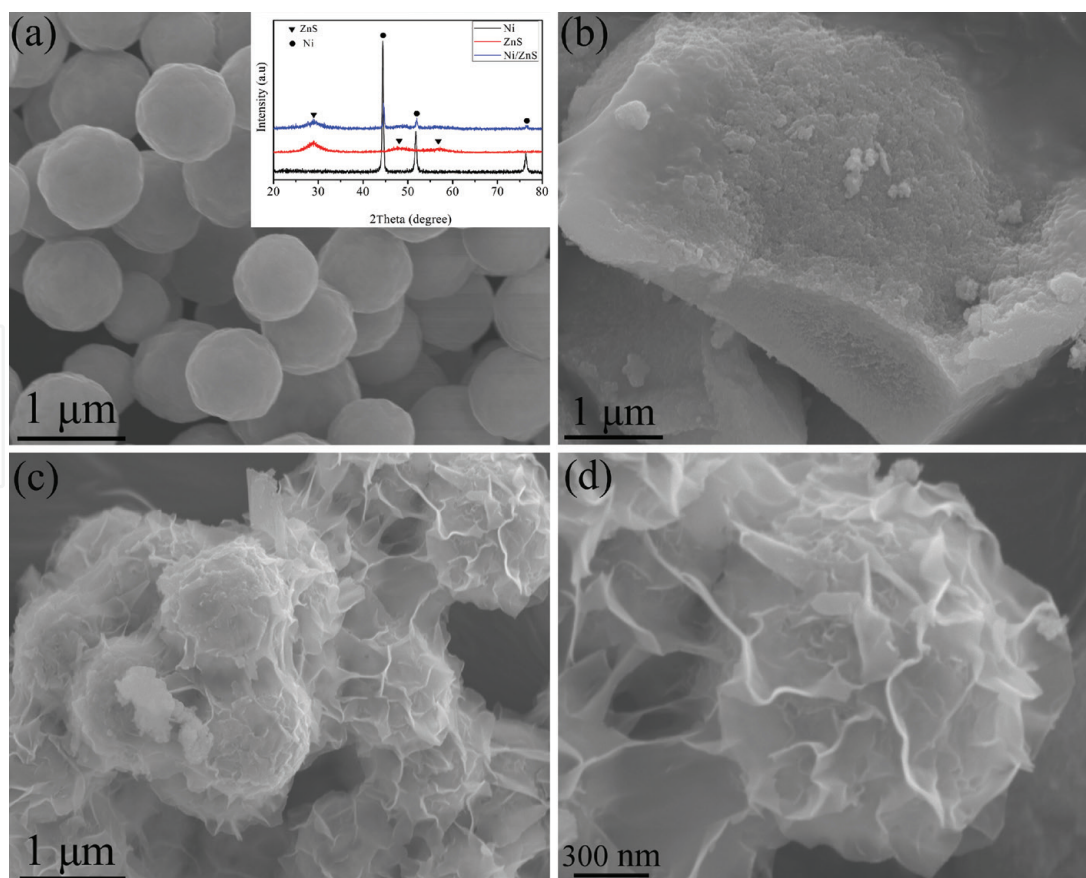


Figure 8. SEM images of (a) Ni microspheres, (b) ZnS particles, and (c, d) the as-prepared Ni/ZnS composites. The inset in (b) is the magnified SEM image of ZnS particles. Inset in Figure 8a is the XRD patterns of Ni microspheres, ZnS particles and Ni/ZnS composites [45] (permission from RSC).

composites is also investigated by XRD measurements. Noticeably, we expectantly observed the diffraction peaks, which are in good accordance with Ni and ZnS, respectively. One can conclude that the as-obtained core/shell structural composites are made up of crystalline Ni and ZnS. **Figure 8a** presents the SEM image of the Ni microspheres. One can notice that the products have a relatively uniform spherical shape with the diameter of 0.7–1.0 μm. The pure ZnS products appear to have irregular shapes (**Figure 8b**). In raw ZnS particles, the formation of ZnS is via a two-step pathway. The fresh nanoparticles incline to aggregate for the sake of decreasing the surface energy. Therefore, we could obtain the irregular gathering ZnS particles. Whereas, as for the Ni/ZnS system, ZnS particles were generated via the template way (heterogeneous nucleation, raw Ni as template). Therefore, the variation of the shape and dimensions of ZnS particles in pure ZnS and core-shell Ni/ZnS composites could be seen. **Figure 8c, d** present the SEM images of core-shell Ni/ZnS. In comparison with pure Ni (**Figure 8a**), one significant distinction is clearly observed between the Ni/ZnS composites and the pure Ni particles. The distinction is that the Ni particles are absolutely wrapped by the ZnS nanowalls. The large-scale SEM image in **Figure 8d** suggests that the as-prepared Ni/ZnS composites show crinkled and rough textures, which are similar with the reduced graphene oxide sheets [46]. The thickness of ZnS nanowall is about 10 nm.

3.1.2 EM properties of core-shell Ni@ZnS composites

The relative complex permittivity (ϵ' and ϵ'') and permeability (μ' and μ'') of the Ni/paraffin, ZnS/paraffin and Ni@ZnS/paraffin composite samples are measured over a frequency of 2–18 GHz. **Figure 9a–c** manifest the real part (ϵ') and imaginary

part (ϵ'') of the complex permittivity as a function of frequency. The ϵ' of Ni/paraffin composite shows a gradual decrease with frequency (**Figure 9a**).

However, the ϵ'' values are relative constant without significant change over the 2–18 GHz. The ϵ' and ϵ'' of ZnS/paraffin composite presents constant value (4.5 and 0.5, respectively) in **Figure 9b**. The ϵ' of the Ni/ZnS composite firstly reduces in the frequency of 2–15 GHz and then improves with increasing frequency (**Figure 9c**). Nevertheless, the ϵ'' exhibits the opposite tendency in the frequency of 2–18 GHz. One can note that the ϵ'' values of Ni/ZnS composite presents a peak in the 13–15 GHz range, which is originated from the natural resonance behavior of core-shell micro-structure [21, 47]. Furthermore, it can be found that the ϵ'' values of Ni/paraffin composite are larger than those of ZnS/paraffin composite and Ni@ZnS/paraffin composite. Based on the free electron theory [17], $\epsilon'' \approx 1/2 \pi \epsilon_0 \rho f$, where ρ is the resistivity. The lower ϵ'' values of ZnS/paraffin composite and Ni@ZnS/paraffin composite indicate the higher electric resistivity. In general, a high electrical resistivity is favorable for improving the microwave absorption abilities [48].

Figure 9 (d–f) present the curves of the real part (μ') and imaginary part (μ'') of the complex permeability as a function of frequency for the Ni/paraffin, ZnS/paraffin and Ni@ZnS/paraffin composites. The μ' and μ'' of Ni/paraffin composite are 0.81–1.59 and 0.05–0.51, respectively (**Figure 9d**). Compared with the complex permittivity (**Figure 9a**), the values of complex permeability is relatively small, which lead to mismatch impedance. The impedance match is required that complex

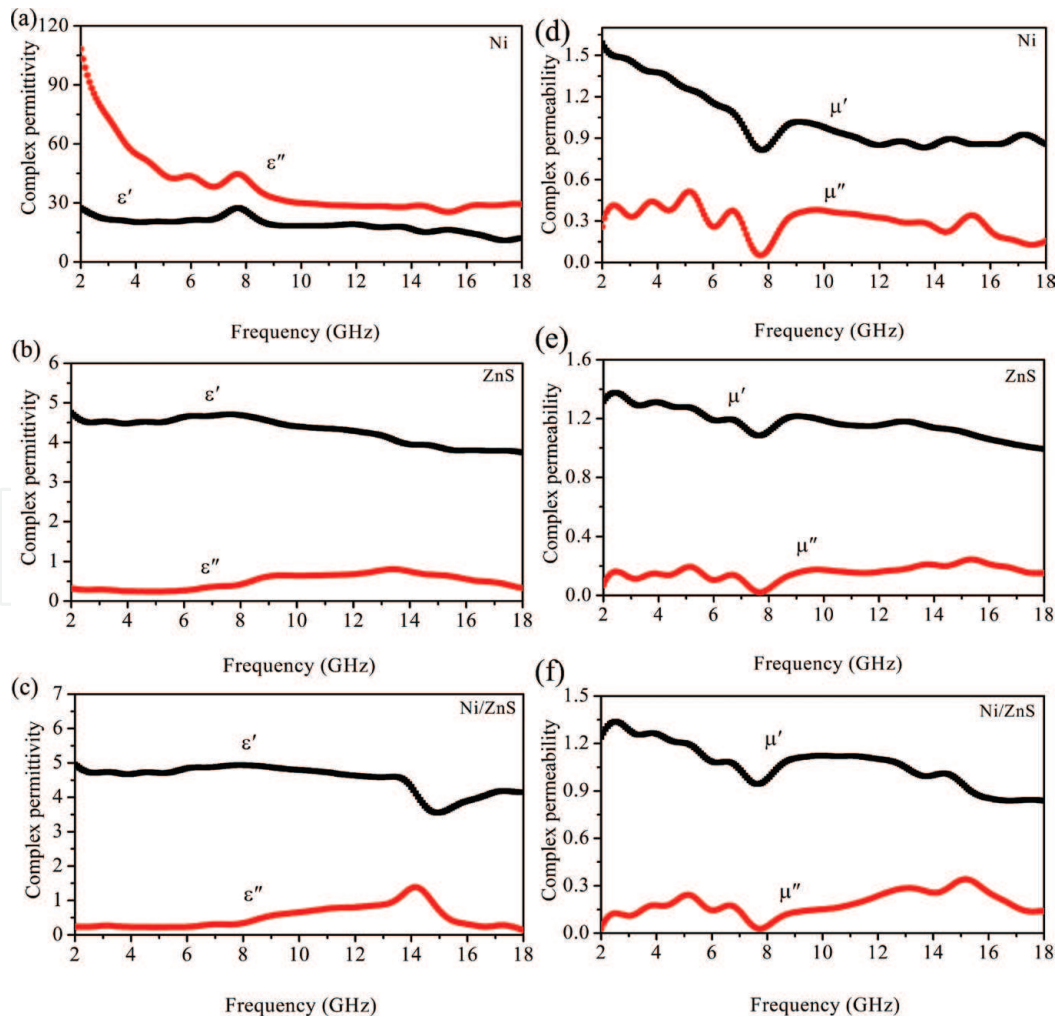


Figure 9. Frequency dependence of the complex permittivity ($\epsilon_r = \epsilon' - j\epsilon''$) of (a) Ni microspheres, (b) ZnS particles, and (c) Ni/ZnS composites; frequency dependence of the complex permeability ($\mu_r = \mu' - j\mu''$) of (d) Ni microspheres, (e) ZnS particles, and (f) Ni/ZnS composites [45] (permission from RSC).

permittivity is close to the permeability, which can make microwaves enter into the materials as much as possible [49]. The higher permittivity of the absorber plays a negative role in the impedance match [50], thus gives rise to inferior microwave absorption. From the **Figure 9e, f**, it can be found that the complex permeability of ZnS/paraffin and Ni@ZnS/paraffin composite exhibit the similar tendency with an increased frequency. The μ' values of 0.99–1.38 and 0.84–1.34 could be observed in ZnS/paraffin and Ni@ZnS/paraffin composites, respectively. The μ'' values are in the range of 0.02–0.24 and 0.03–0.34 for the ZnS/paraffin and Ni@ZnS/paraffin composites, respectively. Given the complex permittivity (**Figure 9b, c**), it can be found that the relation between permittivity and permeability is prone to be close (good impedance match). The good impedance match is beneficial for the microwave absorption. On the basis of the above results, one can deduce that the impedance match of ZnS/paraffin and Ni@ZnS/paraffin is superior to that of Ni/paraffin composite. Thus, the ZnS/paraffin and Ni@ZnS/paraffin composites may possess better dissipation abilities of microwave energy.

It is widely accepted that the RL values could be utilized to evaluate the microwave absorption abilities of EM materials. **Figure 10a** exhibits the calculated RL values of Ni, ZnS and Ni/ZnS paraffin composites with 70 wt% amounts at the thickness of 2.5 mm in the frequency range of 2–18 GHz. Because a paraffin matrix is transparent to microwaves, these results are generally considered as the wave-absorption abilities of the filler itself. It is noting that the microwave absorption properties of Ni particles are weak and the optimal RL value is only -3.04 dB at 5.28 GHz, which is due to the mismatch impedance. Another possible factor is that the skin effect could be observed in Ni microspheres, which is harmful for microwave absorption [30]. Compared with Ni particles, ZnS particles and ZnS nanowall-coated Ni composite presents the superior microwave absorption abilities, which stems from good impedance match. It is worth pointing that, for Ni@ZnS composite, the minimal RL of -20.16 dB is observed at 13.92 GHz and RL values below -10 dB are seen in the 12–16.48 GHz rang. **Figure 10b** displays the relationship between RL and frequency for the paraffin wax composites with 70 wt% Ni/ZnS in various thicknesses. The optimal RL is -25.78 dB at 14.24 GHz with the corresponding thickness of 2.7 mm. The effective absorption (less than -10 dB) bandwidth reaches 4.72 GHz (11.52–16.24 GHz). Interestingly, with increasing the sample thickness, the location of minimal absorption peaks almost keeps the same at various thicknesses without moving to lower frequency, which has also been recorded by other' groups [51]. The location of absorption peaks is in accordance with the natural resonance, which means the resonance behavior in permittivity influences the microwave absorption.

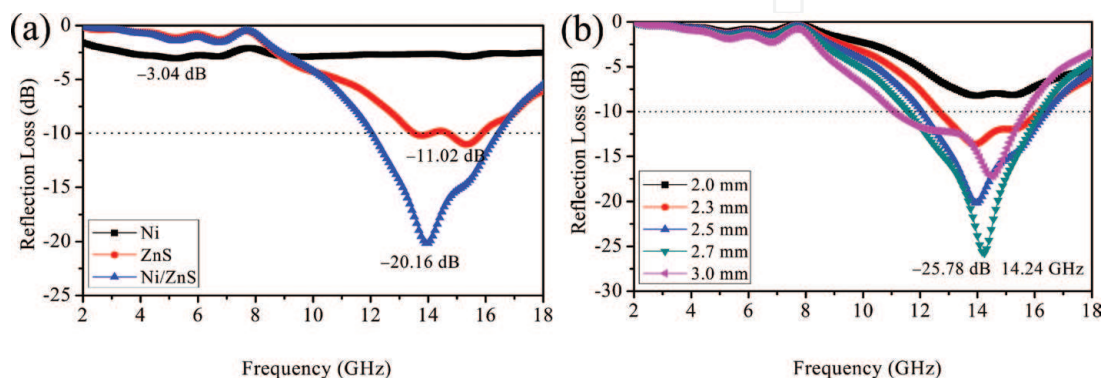


Figure 10.
(a) RL curves of Ni, ZnS and Ni/ZnS paraffin composite with 70 wt% loadings at the thickness of 2.5 mm;
(b) RL curves of 70 wt% Ni/ZnS wax-composite at various thicknesses in the frequency of 2–18 GHz [45]
(permission from RSC).

3.2 Urchin-like ZnS/Ni₃S₂@Ni composites as microwave absorbers

The EM absorption properties of nanomaterial are associated with the size, shape, and dimensionality. Metal sulfide nanomaterials have captured more and more attention due to their excellent properties and wide applications in electronic and optoelectronic devices. Nickel subsulfide and ZnS are the important categories in the metal sulfide family [52, 53] thanks to their various applications such as in lithium ion batteries, supercapacitors, dye-sensitized [54, 55] and charge transfer, anion exchange, electricity generation [56, 57], respectively. Due to the semiconductor properties of nickel subsulfide and ZnS, it can induce dipole and space charge polarizations when placed in the alternated electromagnetic field [16, 58]. Moreover, nickel subsulfide (Ni₃S₂) are highly metallic compared to insulating oxide compounds, which can cause conductive loss [59]. The core-shell Ni@ZnS composites with the improvement of electromagnetic properties were reported by our earlier literatures [45, 60]. To the best of our knowledge, the EM wave absorption of core-shell structured ternary ZnS/Ni₃S₂@Ni composite is hardly found in the published papers. Herein, a novel ZnS/Ni₃S₂@Ni composite with urchin-like core-shell structure is successfully synthesized, and it exhibits the excellent EM absorption and the absorption mechanism of such unique hierarchical microstructure is also discussed in detail.

3.2.1 Preparation of urchin-like ZnS/Ni₃S₂@Ni composites

The monodispersed Ni microspheres were prepared according to our previous literatures [37, 45, 62]. Synthesis of urchin-like core-shell structured ZnS/Ni₃S₂@Ni composite [61]: in brief, Ni (0.05 g) was dispersed in a mixture of aqueous solution of distilled water (30 mL) and ethanol (30 mL) containing 1.0 M NaOH. Then, 1 mmol ZnCl₂ and 2 mmol Na₂S·9H₂O were introduced into above mixture, respectively. The mixture was transferred to a Teflon-lined autoclave. The sealed autoclave was heated to 120°C for 15 h. To explore the possible generation mechanism of core-shell microstructure urchins and effects of temperatures on the shapes of target products, the temperature-control experiments (60°C, 80°C, 100°C and 120°C) were also conducted.

The phase constituent and structure of the as-prepared Ni microspheres and urchin-like ZnS/Ni₃S₂@Ni products are characterized by XRD. **Figure 11a** displays the XRD curve of uncoated Ni microspheres, which could be well assigned to face-centered cubic structure of Ni (JCPDS No. 040850). As presented in **Figure 11b**, except for the diffraction peaks of Ni, the other diffraction peaks could be attributed to the zinc-blende ZnS (JCPDS Card No. 05-0566) and Ni₃S₂ (JCPDS Card No. 76-1870). From these XRD patterns, it can be confirmed that the core-shell ZnS/Ni₃S₂@Ni composite is composed of nickel, nickel sulfide and zinc sulfide. It can be inferred that nickel has functioned as the template for in-situ generation of Ni₃S₂ and deposition of ZnS.

To investigate the morphology of the products, FESEM images are taken for Ni microspheres and ZnS/Ni₃S₂@Ni composite and the corresponding results were shown in **Figure 12**. From the **Figure 12a**, it can be seen that Ni products were composed of uniform distribution and smooth surface of microspheres. **Figure 12b, c** presents the different magnification FESEM images of core-shell ZnS/Ni₃S₂@Ni composite. Interestingly, from panoramic observation (**Figure 12b**), urchin-like products are optionally grown on the surfaces of Ni microspheres and the outline of Ni spheres cannot be clearly observed due to the formation of ZnS/Ni₃S₂. Noticeably, the decrease size of Ni particles could be observed, which suggests the depletion of Ni products. The thorns possess about 1 μm and 50 nm in length and

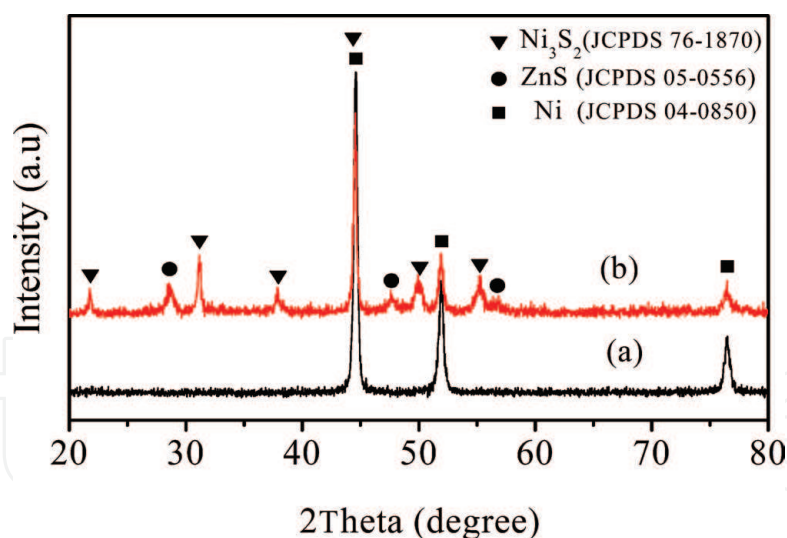


Figure 11. XRD patterns of (a) pristine Ni microspheres and (b) as-prepared ZnS/Ni₃S₂@Ni [61] (permission from RSC).

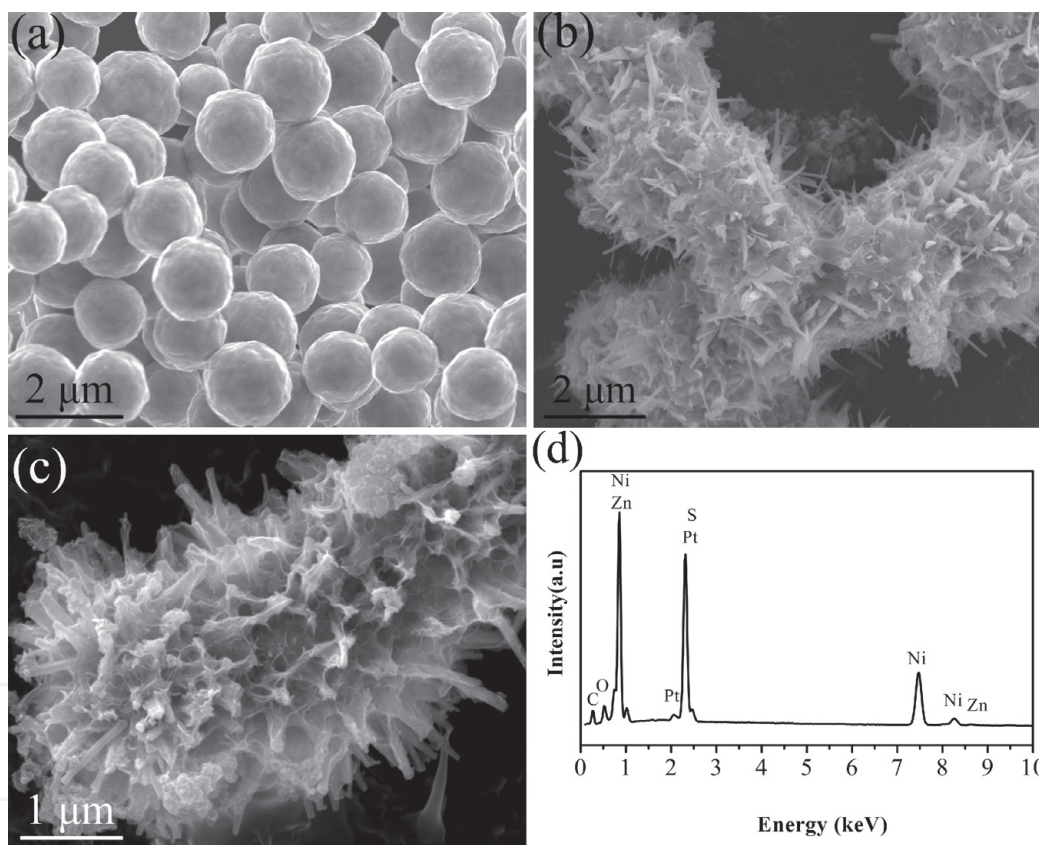


Figure 12. FESEM images of (a) Ni microspheres, (b, c) urchin-like core-shell structured ZnS/Ni₃S₂@Ni composite, and (d) EDS profile of ZnS/Ni₃S₂@Ni composite [61] (permission from RSC).

diameter, respectively. Further observation from the high magnification FESEM image (**Figure 12c**), the existence of crumple products encircle Ni particles and the crinkled products are expected to be linked between Ni particles and thorns. **Figure 12d** presents the EDS of the ZnS/Ni₃S₂@Ni composite. The EDS reveals the presence of elements of S, Zn and Ni. Pt peaks are also seen in the EDS curve because the SEM sample is prepared by sputtering of platinum onto the sample.

It is assumed that the reaction temperature has an effect on the morphology of core-shell heterostructure. At low temperature (60°C), interestingly, there are plentiful waxberry-like products existed in **Figure 13a**. It is due to the fact that Ni

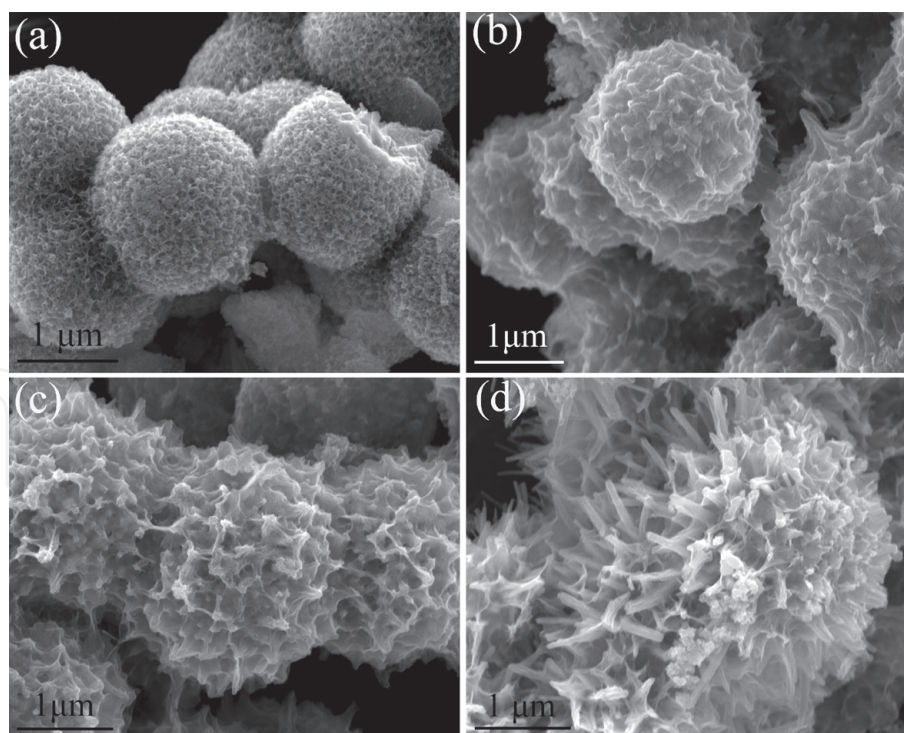


Figure 13. FESEM images of core-shell $\text{ZnS}/\text{Ni}_3\text{S}_2@\text{Ni}$ composites prepared at various reaction temperatures: (a) 60°C , (b) 80°C , (c) 100°C , and (d) 120°C [61] (permission from RSC).

microspheres were coated by wrinkle ZnS products. Ni_3S_2 nanoparticles are in-situ formed by depletion of Ni particles and then covered on the surface of left Ni products. With elevating the reaction temperatures to high temperatures (80°C), one can notice that some protuberant prickles were grown on the surfaces of core-shell composites (**Figure 13b**). When the reaction temperature is increased to 100°C , the presence of more and strong protuberant stabs on the crumple surfaces of composite can be obviously observed (**Figure 13c**). With further enhancing the temperature to 120°C , the target urchin-like core-shell structural $\text{ZnS}/\text{Ni}_3\text{S}_2@\text{Ni}$ composites are formed with numerous of thorns or rods grown on the rugged surfaces (**Figure 13d**).

3.2.2 EM properties of urchin-like $\text{ZnS}/\text{Ni}_3\text{S}_2@\text{Ni}$ composites

With the purpose of revealing the electromagnetic wave absorption properties, the representation RL values of the core-shell $\text{ZnS}/\text{Ni}_3\text{S}_2@\text{Ni}$ paraffin-composites with different sample thicknesses are simulated. **Figure 14** reveals the RL values of the core-shell $\text{ZnS}/\text{Ni}_3\text{S}_2@\text{Ni}$ composites prepared at different temperatures with thickness varies from 0.8 to 2.5 mm in the frequency range of 1–18 GHz. It can be found that urchin-like $\text{ZnS}/\text{Ni}_3\text{S}_2@\text{Ni}$ composite exhibits outstanding electromagnetic absorption. The minimal RL is down to -27.6 dB at 5.2 GHz as the thickness is 2.5 mm. Notably, the reflection loss of urchin-like $\text{ZnS}/\text{Ni}_3\text{S}_2@\text{Ni}$ is -21.6 dB at 13.3 GHz with the absorber thickness of 1.0 mm, and the valuable bandwidth (RL below -10 dB) could reach 2.5 GHz (12.2–14.7 GHz), which is better than those of the literatures about microwave absorption performances of dielectric/magnetic composites, such as $\text{Fe}@\text{SnO}_2$ (> -10 dB) [63], and Co/CoO (-14.5 dB) [64]. Meanwhile, the absorption peaks would move to lower frequencies and dual RL peaks could be obtained with an increased absorber thickness above 2.5 mm. This phenomenon could be described by the quarter-wavelength cancelation model [65].

According to above results, we propose a possible electromagnetic wave absorption mechanism for the core-shell $\text{ZnS}/\text{Ni}_3\text{S}_2@\text{Ni}$ heterogeneous system. When the

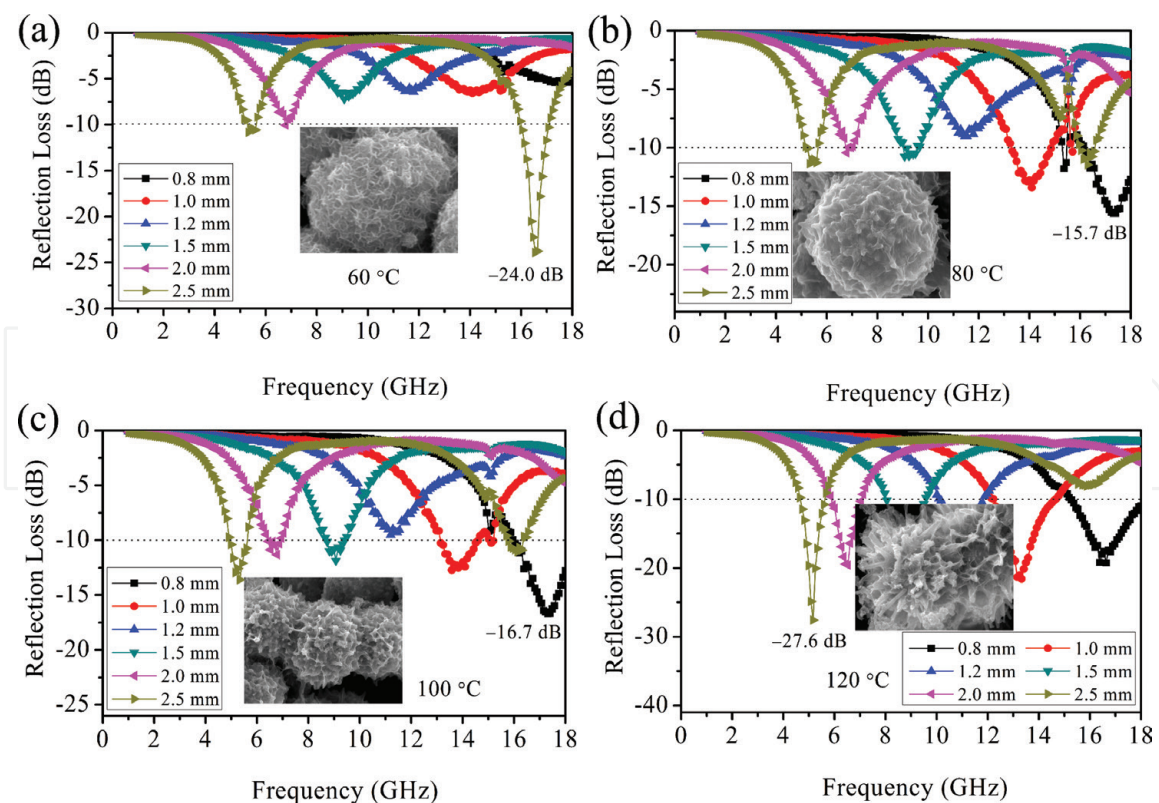


Figure 14.

The calculated RL of core-shell $\text{ZnS}/\text{Ni}_3\text{S}_2@\text{Ni}$ composites prepared at various temperatures: (a) 60°C , (b) 80°C , (c) 100°C , and (d) 120°C with different thickness in the frequency range of 1–18 GHz [61] (permission from RSC).

$\text{ZnS}/\text{Ni}_3\text{S}_2@\text{Ni}$ composite is subjected to EM wave radiation, the Ni_3S_2 thorns grown on the surfaces of Ni microspheres are expected as antenna receiver to allow electromagnetic waves penetrate into interior of absorber as much as possible, namely called good impedance match [66, 67]. Moreover, EM absorption is also understood from the viewpoint of Ohmic heating induced by an alternating magnetic field [68], in which $\text{ZnS}/\text{Ni}_3\text{S}_2@\text{Ni}$ composite with relatively high electric conductivity. Thirdly, due to the heterogeneous systems of core-shell $\text{ZnS}/\text{Ni}_3\text{S}_2@\text{Ni}$ composites, the multi-interfaces between the ZnS, Ni_3S_2 , and Ni are favorable for improvement of electromagnetic wave absorption thanks to the interaction between electromagnetic radiation and charged multipoles at the interfaces [69]. The interfacial polarizations [42, 70] occurring at the interfaces are resulted from the migration of charge carriers through different conductivity properties of the composite material. During the irradiated by alternating electromagnetic field, an additional interfacial relaxation is produced, which is beneficial for the electromagnetic absorption [71]. On the other hand, the cooperation effect between dielectric loss at high frequency and magnetic loss at low frequency contribute to the improvement of electromagnetic absorption [72].

4. Conclusion

Various morphologies of Ni/ZnO composites are successfully fabricated by a hydrothermal method. The shapes of ZnO nanostructures could be effectively monitored by tuning the contents of $\text{NH}_3\cdot\text{H}_2\text{O}$. One can find that the morphology of ZnO plays an important role on the microwave absorption capabilities. The core-shell structural Ni/polyhedron ZnO presents relatively high dielectric loss, magnetic loss and microwave dissipation abilities compared with the other Ni/ZnO samples.

The minimal RL could reach -48.6 dB at 13.4 GHz in the absorber thickness of 2.0 mm. The absorption band with RL below -10 dB could reach 6.0 GHz between 10.5 and 16.5 GHz. The enhanced microwave dissipation abilities are attributed to the synergetic effect between dielectric loss and magnetic loss, strong dissipation ability, as well as the multiple polarization of the core/shell interfaces.

The hierarchical Ni-CuO heterostructures have been successfully synthesized by a two-step process. The as-prepared Ni-CuO products display a rice-like coating composite. Moreover, by tuning the molar ratio of $\text{CuCl}_2 \cdot 2\text{H}_2\text{O}$ to the Ni microspheres, different shapes and coverage densities of CuO coating are obtained. The effects of CuO amounts on the Ni microspheres for microwave absorption properties have been investigated. The thin CuO-coated Ni composites (S-1) exhibit the enhanced electromagnetic absorption properties. The optimal RL is -62.2 dB at 13.8 GHz with only thickness of 1.7 mm. The outstanding microwave absorption properties result from the strongest attenuation constant, interfacial polarization of and the synergetic effect between the dielectric loss and magnetic loss.

ZnS nanowall-covered Ni composite is fabricated via a hydrothermal template method. The as-obtained Ni/ZnS composites display the crumble and rough features and the thickness of ZnS nanowall is about 10 nm. In comparison with raw Ni and ZnS particles, the Ni@ZnS composites show superior microwave dissipation abilities. The optimal RL of -25.78 dB could be obtained at 14.24 GHz and the valuable (less than -10 dB) band could reach 4.72 GHz (11.52–16.24 GHz) in the thickness of 2.7 mm. Moreover, the location of absorption peaks is almost similar at various thicknesses without moving to low frequency, which originates from natural resonance in permittivity.

Novel and interesting urchin-like ZnS/Ni₃S₂@Ni composites are synthesized through a two-step process including solution reduction and subsequently a template method. Crucially, the morphologies of the core-shell ZnS/Ni₃S₂@Ni composites are determined by the reaction temperature. Different ZnS/Ni₃S₂@Ni composites prepared at different temperatures show variable electromagnetic absorption responses, for which the urchin-like ZnS/Ni₃S₂@Ni obtained at 120°C show the enhanced EM absorption properties thanks to its promising dielectric loss and magnetic loss, good impedance match, as well as its unique urchin-like structure. Multiple dielectric resonances stemming from effective accumulation of different polarizations in the urchin-like structure are regarded to make a contribution to the enhancement of electromagnetic wave absorption. It is believed that *in situ* synthesis of core-shell ZnS/Ni₃S₂@Ni composites may open up a new avenue for the design and preparation of novel microwave absorbers with promising application potential.

In a word, the core-shell configuration is proved to be a promising pathway to design high-efficiency EM absorption properties of Ni based composites.

Conflict of interest

There are no conflicts to declare.

IntechOpen

Author details

Biao Zhao^{1,2*} and Rui Zhang^{1,3}

1 Henan Key Laboratory of Aeronautical Materials and Application Technology, School of Material Science and Engineering, Zhengzhou University of Aeronautics, Zhengzhou, Henan, China

2 Department of Mechanical and Industrial Engineering, University of Toronto, Toronto, Ontario, Canada

3 School of Material Science and Engineering, Zhengzhou University, Zhengzhou, Henan, China

*Address all correspondence to: zhaobiao1813@163.com

IntechOpen

© 2018 The Author(s). Licensee IntechOpen. This chapter is distributed under the terms of the Creative Commons Attribution License (<http://creativecommons.org/licenses/by/3.0>), which permits unrestricted use, distribution, and reproduction in any medium, provided the original work is properly cited. 

References

- [1] Jian X, Wu B, Wei Y, Dou SX, Wang X, He W, et al. Facile synthesis of $\text{Fe}_3\text{O}_4/\text{GCs}$ composites and their enhanced microwave absorption properties. *ACS Applied Materials & Interfaces*. 2016;**8**(9):6101-6109. DOI: 10.1021/acscami.6b00388
- [2] Lv H, Guo Y, Yang Z, Cheng Y, Wang LP, Zhang B, et al. A brief introduction to the fabrication and synthesis of graphene based composites for the realization of electromagnetic absorbing materials. *Journal of Materials Chemistry C*. 2017;**5**(3):491-512. DOI: 10.1039/C6TC03026B
- [3] Zhao B, Deng J, Zhang R, liang L, Fan B, Bai Z, et al. Recent advances on the electromagnetic wave absorption properties of Ni based materials. *Engineered Science*. 2018;**3**:5-40. DOI: 10.30919/es8d735
- [4] Wang G, Gao Z, Tang S, Chen C, Duan F, Zhao S, et al. Microwave absorption properties of carbon nanocoils coated with highly controlled magnetic materials by atomic layer deposition. *ACS Nano*. 2012;**6**(12):11009-11017. DOI: 10.1021/nn304630h
- [5] Ye F, Song Q, Zhang Z, Li W, Zhang S, Yin X, et al. Direct growth of edge-rich graphene with tunable dielectric properties in porous Si_3N_4 ceramic for broadband high-performance microwave absorption. *Advanced Functional Materials*. 2018;**28**(17):1707205. DOI: 10.1002/adfm.201707205
- [6] Liu Q, Cao Q, Bi H, Liang C, Yuan K, She W, et al. $\text{CoNi@SiO}_2\text{@TiO}_2$ and CoNi@Air@TiO_2 microspheres with strong wideband microwave absorption. *Advanced Materials*. 2016;**28**(3):486-490. DOI: 10.1002/adma.201503149
- [7] Zhang Y, Huang Y, Zhang T, Chang H, Xiao P, Chen H, et al. Broadband and tunable high-performance microwave absorption of an ultralight and highly compressible graphene foam advanced materials. 2015;**27**(12):2049-2053. DOI: 10.1002/adma.201405788
- [8] Xi L, Wang Z, Zuo Y, Shi X. The enhanced microwave absorption property of CoFe_2O_4 nanoparticles coated with a $\text{Co}_3\text{Fe}_7\text{-Co}$ nanoshell by thermal reduction. *Nanotechnology*. 2011;**22**(4):045707. DOI: 10.1088/0957-4484/22/4/045707
- [9] Zhou W, Hu X, Bai X, Zhou S, Sun C, Yan J, et al. Synthesis and electromagnetic, microwave absorbing properties of Core-Shell $\text{Fe}_3\text{O}_4\text{-Poly}(3, 4\text{-ethylenedioxythiophene})$ microspheres. *ACS Applied Materials & Interfaces*. 2011;**3**(10):3839-3845. DOI: 10.1021/am2004812
- [10] Chen Y-J, Zhang F, G-g Z, X-y F, Jin H-B, Gao P, et al. Synthesis, multi-nonlinear dielectric resonance, and excellent electromagnetic absorption characteristics of $\text{Fe}_3\text{O}_4/\text{ZnO}$ core/shell nanorods. *The Journal of Physical Chemistry C*. 2010;**114**(20):9239-9244. DOI: 10.1021/jp912178q
- [11] Liu J, Che R, Chen H, Zhang F, Xia F, Wu Q, et al. Microwave absorption enhancement of multifunctional composite microspheres with spinel Fe_3O_4 cores and anatase TiO_2 shells. *Small*. 2012;**8**(8):1214-1221. DOI: 10.1002/sml.201102245
- [12] Zhu C-L, Zhang M-L, Qiao Y-J, Xiao G, Zhang F, Chen Y-J. $\text{Fe}_3\text{O}_4/\text{TiO}_2$ core/shell nanotubes: synthesis and magnetic and electromagnetic wave absorption characteristics. *The Journal of Physical Chemistry C*. 2010;**114**(39):16229-16235. DOI: 10.1021/jp104445m
- [13] Metin Ö, Mazumder V, Özkaz S, Sun S. Monodisperse nickel nanoparticles and their catalysis in

- hydrolytic dehydrogenation of ammonia borane. *Journal of the American Chemical Society*. 2010;**132**(5):1468-1469. DOI: 10.1021/ja909243z
- [14] Xiong J, Shen H, Mao J, Qin X, Xiao P, Wang X, et al. Porous hierarchical nickel nanostructures and their application as a magnetically separable catalyst. *Journal of Materials Chemistry*. 2012;**22**(24):11927-11932. DOI: 10.1039/C2JM30361B
- [15] Zhao B, Shao G, Fan B, Li W, Pian X, Zhang R. Enhanced electromagnetic wave absorption properties of Ni-SnO₂ core-shell composites synthesized by a simple hydrothermal method. *Materials Letters*. 2014;**121**:118-121. DOI: 10.1016/j.matlet.2014.01.081
- [16] Wang H, Guo H, Dai Y, Geng D, Han Z, Li D, et al. Optimal electromagnetic-wave absorption by enhanced dipole polarization in Ni/C nanocapsules. *Applied Physics Letters*. 2012;**101**(8):083116. DOI: 10.1063/1.4747811
- [17] Liu XG, Jiang JJ, Geng DY, Li BQ, Han Z, Liu W, et al. Dual nonlinear dielectric resonance and strong natural resonance in Ni/ZnO nanocapsules. *Applied Physics Letters*. 2009;**94**(5):053119. DOI: 10.1063/1.3079393
- [18] Liu X, Feng C, Or SW, Jin C, Xiao F, Xia A, et al. Synthesis and electromagnetic properties of Al/AlO_x-coated Ni nanocapsules. *Materials Research Bulletin*. 2013;**48**(10):3887-3891. DOI: 10.1016/j.materresbull.2013.05.110
- [19] Wang B, Zhang J, Wang T, Qiao L, Li F. Synthesis and enhanced microwave absorption properties of Ni@Ni₂O₃ core-shell particles. *Journal of Alloys and Compounds*. 2013;**567**:21-25. DOI: 10.1016/j.jallcom.2013.03.028
- [20] Dong XL, Zhang XF, Huang H, Zuo F. Enhanced microwave absorption in Ni/polyaniline nanocomposites by dual dielectric relaxations. *Applied Physics Letters*. 2008;**92**(1):013127. DOI: 10.1063/1.2830995
- [21] Liu X, Feng C, Or SW, Sun Y, Jin C, Li W, et al. Investigation on microwave absorption properties of CuO/Cu₂O-coated Ni nanocapsules as wide-band microwave absorbers. *RSC Advances*. 2013;**3**(34):14590-14594. DOI: 10.1039/C3RA40937F
- [22] Li H, Huang Y, Sun G, Yan X, Yang Y, Wang J, et al. Directed growth and microwave absorption property of crossed ZnO netlike micro-/nanostructures. *The Journal of Physical Chemistry C*. 2010;**114**(22):10088-10091. DOI: 10.1021/jp100341h
- [23] Zhao B, Shao G, Fan B, Guo W, Xie Y, Zhang R. Facile synthesis of Ni/ZnO composite: Morphology control and microwave absorption properties. *Journal of Magnetism and Magnetic Materials*. 2015;**382**:78-83. DOI: 10.1016/j.jmmm.2015.01.053
- [24] Wang ZL, Kong XY, Zuo JM. Induced growth of asymmetric nanocantilever arrays on polar surfaces. *Physical Review Letters*. 2003;**91**(18):185502. DOI: 10.1103/PhysRevLett.91.185502
- [25] Yan J-F, Zhang Z-Y, You T-G, Zhao W, Yun J-N, Zhang F-C. Effect of polyacrylamide on morphology and electromagnetic properties of chrysanthemum-like ZnO particles. *Chinese Physics B*. 2009;**18**(10):4552. DOI: 10.1088/1674-1056/18/10/076
- [26] Na J-S, Gong B, Scarel G, Parsons GN. Surface polarity shielding and hierarchical ZnO nano-architectures produced using sequential hydrothermal crystal synthesis and thin film atomic layer deposition. *ACS Nano*.

2009;**3**(10):3191-3199. DOI: 10.1021/nn900702e

[27] Jung S-H, Oh E, Lee K-H, Yang Y, Park CG, Park W, et al. Sonochemical preparation of shape-selective ZnO nanostructures. *Crystal Growth & Design*. 2007;**8**(1):265-269. DOI: 10.1021/cg070296l

[28] Flaifel MH, Ahmad SH, Abdullah MH, Rasid R, Shaari AH, El-Saleh AA, Appadu S. Preparation, thermal, magnetic and microwave absorption properties of thermoplastic natural rubber matrix impregnated with NiZn ferrite nanoparticles. *Composites Science and Technology*. 2014;**96**:103-108

[29] Li G, Xie T, Yang S, Jin J, Jiang J. Microwave absorption enhancement of porous carbon fibers compared with carbon nanofibers. *The Journal of Physical Chemistry C*. 2012;**116**(16):9196-9201. DOI: 10.1021/jp300050u

[30] Cooper ER, Andrews CD, Wheatley PS, Webb PB, Wormald P, Morris RE. Ionic liquids and eutectic mixtures as solvent and template in synthesis of zeolite analogues. *Nature*. 2004;**430**(7003):1012-1016. DOI: 10.1038/nature02860

[31] Zhang X, Dong X, Huang H, Lv B, Lei J, Choi C. Microstructure and microwave absorption properties of carbon-coated iron nanocapsules. *Journal of Physics D: Applied Physics*. 2007;**40**(17):5383. DOI: 10.1088/0022-3727/40/17/056

[32] Yan S, Zhen L, Xu C, Jiang J, Shao W. Microwave absorption properties of FeNi₃ submicrometre spheres and SiO₂@ FeNi₃ core-shell structures. *Journal of Physics D: Applied Physics*. 2010;**43**(24):245003. DOI: 10.1088/0022-3727/43/24/245003

[33] Pecquenard B, Le Cras F, Poinot D, Sicardy O, Manaud J-P. Thorough

characterization of sputtered CuO thin films used as conversion material electrodes for lithium batteries. *ACS Applied Materials & Interfaces*. 2014;**6**(5):3413-3420. DOI: 10.1021/am4055386

[34] Kargar A, Jing Y, Kim SJ, Riley CT, Pan X, Wang D. ZnO/CuO Heterojunction branched nanowires for photoelectrochemical hydrogen generation. *ACS Nano*. 2013;**7**(12):11112-11120. DOI: 10.1021/nn404838n

[35] Zeng J, Xu J, Tao P, Hua W. Ferromagnetic and microwave absorption properties of copper oxide-carbon fiber composites. *Journal of Alloys and Compounds*. 2009;**487**(1-2):304-308. DOI: 10.1016/j.jallcom.2009.07.112

[36] Jun Z, Huiqing F, Yangli W, Shiquan Z, Jun X, Xinying C. Ferromagnetic and microwave absorption properties of copper oxide/cobalt/carbon fiber multilayer film composites. *Thin Solid Films*. 2012;**520**(15):5053-5059. DOI: 10.1016/j.tsf.2012.03.059

[37] Zhao B, Shao G, Fan B, Zhao W, Zhang R. Facile synthesis and enhanced microwave absorption properties of novel hierarchical heterostructures based on a Ni microsphere-CuO nano-rice core-shell composite. *Physical Chemistry Chemical Physics*. 2015;**17**(8):6044-6052. DOI: 10.1039/C4CP05229C

[38] Wang Z, Wu L, Zhou J, Cai W, Shen B, Jiang Z. Magnetite nanocrystals on multiwalled carbon nanotubes as a synergistic microwave absorber. *The Journal of Physical Chemistry C*. 2013;**117**(10):5446-5452. DOI: 10.1021/jp4000544

[39] Pan G, Zhu J, Ma S, Sun G, Yang X. Enhancing the electromagnetic performance of Co through the phase-controlled synthesis of hexagonal

and cubic Co nanocrystals grown on graphene. *ACS Applied Materials & Interfaces*. 2013;5(23):12716-12724. DOI: 10.1021/am404117v

[40] Wang C, Han X, Zhang X, Hu S, Zhang T, Wang J, et al. Controlled synthesis and morphology-dependent electromagnetic properties of hierarchical cobalt assemblies. *The Journal of Physical Chemistry C*. 2010;114(35):14826-14830. DOI: 10.1021/jp1050386

[41] Ortega N, Kumar A, Katiyar R, Rinaldi C. Dynamic magneto-electric multiferroics PZT/CFO multilayered nanostructure. *Journal of Materials Science*. 2009;44(19):5127-5142. DOI: 10.1007/s10853-009-3635-0

[42] Wen S, Liu Y, Zhao X, Cheng J, Li H. Synthesis, multi-nonlinear dielectric resonance and electromagnetic absorption properties of hcp-cobalt particles. *Journal of Magnetism and Magnetic Materials*. 2014;354:7-11. DOI: 10.1016/j.jmmm.2013.10.030

[43] Yan C, Xue D. Room temperature fabrication of hollow ZnS and ZnO architectures by a sacrificial template route. *The Journal of Physical Chemistry B*. 2006;110(114):7102-7106

[44] Gu F, Li CZ, Wang SF, Lü MK. Solution-phase synthesis of spherical zinc sulfide nanostructures. solution-phase synthesis of spherical zinc sulfide nanostructures. *Langmuir*. 2005;22(3):1329-1332

[45] Zhao B, Shao G, Fan B, Zhao W, Xie Y, Zhang R. ZnS nanowall coated Ni composites: facile preparation and enhanced electromagnetic wave absorption. *RSC Advances*. 2014;4(105):61219-61225. DOI: 10.1039/C4RA08095E

[46] Wang G-S, Wu Y, Wei Y-Z, Zhang X-J, Li Y, Li L-D, et al. Fabrication of Reduced Graphene Oxide (RGO)/

Co₃O₄ nanohybrid particles and a RGO/Co₃O₄/Poly(vinylidene fluoride) composite with enhanced wave-absorption properties. *ChemPlusChem*. 2014;79(3):375-381. DOI: 10.1002/cplu.201300345

[47] Ren Y, Zhu C, Zhang S, Li C, Chen Y, Gao P, et al. Three-dimensional SiO₂@Fe₃O₄ core/shell nanorod array/graphene architecture: synthesis and electromagnetic absorption properties. *Nanoscale*. 2013;5(24):12296-12303. DOI: 10.1039/C3NR04058E

[48] Liu XG, Geng DY, Zhang ZD. Microwave-absorption properties of FeCo microspheres self-assembled by Al₂O₃-coated FeCo nanocapsules. *Applied Physics Letters*. 2008;92(24):243110. DOI: 10.1063/1.2945639

[49] Du Y, Liu T, Yu B, Gao H, Xu P, Wang J, et al. The electromagnetic properties and microwave absorption of mesoporous carbon. *Materials Chemistry and Physics*. 2012;135(2-3):884-891. DOI: 10.1016/j.matchemphys.2012.05.074

[50] He S, Wang G-S, Lu C, Liu J, Wen B, Liu H, et al. Enhanced wave absorption of nanocomposites based on the synthesized complex symmetrical CuS nanostructure and poly(vinylidene fluoride). *Journal of Materials Chemistry A*. 2013;1(15):4685-4692. DOI: 10.1039/C3TA00072A

[51] Li Y, Zhang J, Liu Z, Liu M, Lin H, Che R. Morphology-dominant microwave absorption enhancement and electron tomography characterization of CoO self-assembly 3D nano-flowers. *Journal of Materials Chemistry C*. 2014;2(26):5216-5222. DOI: 10.1039/C4TC00739E

[52] Lee CW, Seo S-D, Park HK, Park S, Song HJ, Kim D-W, et al. High-area-capacity lithium storage of the Kirkendall effect-driven hollow hierarchical NiS_x nanoarchitecture.

Nanoscale. 2015;7(6):2790-2796. DOI: 10.1039/C4NR05942E

[53] Huang X, Willinger M-G, Fan H, Xie Z-l, Wang L, Klein-Hoffmann A, et al. Single crystalline wurtzite ZnO/zinc blende ZnS coaxial heterojunctions and hollow zinc blende ZnS nanotubes: synthesis, structural characterization and optical properties. *Nanoscale*. 2014;6(15):8787-8795. DOI: 10.1039/C4NR01575D

[54] Liao Y, Pan K, Pan Q, Wang G, Zhou W, Fu H. In situ synthesis of a NiS/Ni₃S₂ nanorod composite array on Ni foil as a FTO-free counter electrode for dye-sensitized solar cells. *Nanoscale*. 2015;7(5):1623-1626. DOI: 10.1039/C4NR06534D

[55] Wang Z, Li X, Yang Y, Cui Y, Pan H, Wang Z, et al. Highly dispersed [small beta]-NiS nanoparticles in porous carbon matrices by a template metal-organic framework method for lithium-ion cathode. *Journal of Materials Chemistry A*. 2014;2(21):7912-7916. DOI: 10.1039/C4TA00367E

[56] Xitao W, Rong L, Kang W. Synthesis of ZnO@ZnS-Bi₂S₃ core-shell nanorod grown on reduced graphene oxide sheets and its enhanced photocatalytic performance. *Journal of Materials Chemistry A*. 2014;2(22):8304-8313. DOI: 10.1039/C4TA00696H

[57] Zhu Y-P, Li J, Ma T-Y, Liu Y-P, Du G, Yuan Z-Y. Sonochemistry-assisted synthesis and optical properties of mesoporous ZnS nanomaterials. *Journal of Materials Chemistry A*. 2014;2(4):1093-1101. DOI: 10.1039/C3TA13636A

[58] Zhang Q, Li C, Chen Y, Han Z, Wang H, Wang Z, et al. Effect of metal grain size on multiple microwave resonances of Fe/TiO₂ metal-semiconductor composite. *Applied Physics Letters*. 2010;97(13):133115. DOI: 10.1063/1.3496393

[59] Watts PCP, Hsu WK, Barnes A, Chambers B. High permittivity from defective multiwalled carbon nanotubes in the x-band. *Advanced Materials*. 2003;15(7-8):600-603. DOI: 10.1002/adma.200304485

[60] Zhao B, Shao G, Fan B, Zhao W, Chen Y, Zhang R. Facile synthesis of crumpled ZnS net-wrapped Ni walnut spheres with enhanced microwave absorption properties. *RSC Advances*. 2015;5(13):9806-9814. DOI: 10.1039/C4RA15411H

[61] Zhao B, Shao G, Fan B, Zhao W, Zhang S, Guan K, et al. In situ synthesis of novel urchin-like ZnS/Ni₃S₂@Ni composite with a core-shell structure for efficient electromagnetic absorption. *Journal of Materials Chemistry C*. 2015;3(41):10862-10869. DOI: 10.1039/C5TC02063H

[62] Zhao B, Shao G, Fan B, Zhao W, Zhang R. Fabrication and enhanced microwave absorption properties of Al₂O₃ nanoflake-coated Ni core-shell composite microspheres. *RSC Advances*. 2014;4(101):57424-57429. DOI: 10.1039/C4RA10638E

[63] Liu X, Zhou G, Or SW, Sun Y. Fe/amorphous SnO₂ core-shell structured nanocapsules for microwave absorptive and electrochemical performance. *RSC Advances*. 2014;4(93):51389-51394. DOI: 10.1039/C4RA08998G

[64] Wang Z, Bi H, Wang P, Wang M, Liu Z, Shen L, et al. Magnetic and microwave absorption properties of self-assemblies composed of core-shell cobalt-cobalt oxide nanocrystals. *Physical Chemistry Chemical Physics*. 2015;17(5):3796-3801. DOI: 10.1039/C4CP04985C

[65] Li G, Wang L, Li W, Ding R, Xu Y. CoFe₂O₄ and/or Co₃Fe₇ loaded porous activated carbon balls as a lightweight microwave absorbent. *Physical Chemistry Chemical Physics*.

2014;**16**(24):12385-12392. DOI: 10.1039/C4TA05718J

[66] Li X, Feng J, Du Y, Bai J, Fan H, Zhang H, et al. One-pot synthesis of CoFe₂O₄/graphene oxide hybrids and their conversion into FeCo/graphene hybrids for lightweight and highly efficient microwave absorber. *Journal of Materials Chemistry A*. 2015;**3**(10):5535-5546. DOI: 10.1039/C4TA05718J

[67] Tong G, Yuan J, Wu W, Hu Q, Qian H, Li L, et al. Flower-like Co superstructures: Morphology and phase evolution mechanism and novel microwave electromagnetic characteristics. *CrystEngComm*. 2012;**14**(6):2071-2079. DOI: 10.1039/C2CE05910J

[68] Jiang J, Li D, Li S, Wang Z, Wang Y, He J, et al. Electromagnetic wave absorption and dielectric-modulation of metallic perovskite lanthanum nickel oxide. *RSC Advances*. 2015;**19**(19):14584-14591. DOI: 10.1039/C5RA00139K

[69] Yang H-J, Cao W-Q, Zhang D-Q, Su T-J, Shi H-L, Wang W-Z, et al. Hierarchical nanorings on SiC: Enhancing relaxation to tune microwave absorption at elevated temperature. *ACS Applied Materials & Interfaces*. 2015;**7**(13):7073-7077. DOI: 10.1021/acsami.5b01122

[70] Liu Q, Zhang D, Fan T. Electromagnetic wave absorption properties of porous carbon/Co nanocomposites. *Applied Physics Letters*. 2008;**93**(1):013110. DOI: 10.1063/1.2957035

[71] Zhao B, Shao G, Fan B, Zhao W, Xie Y, Zhang R. Synthesis of flower-like CuS hollow microspheres based on nanoflakes self-assembly and their microwave absorption properties. *Journal of Materials Chemistry A*. 2015;**3**(19):10345-10352. DOI: 10.1039/C5TA00086F

[72] Wang Q, Lei Z, Chen Y, Ouyang Q, Gao P, Qi L, et al. Branched polyaniline/molybdenum oxide organic/inorganic heteronanostructures: Synthesis and electromagnetic absorption properties. *Journal of Materials Chemistry A*. 2013;**1**(38):11795-11801. DOI: 10.1039/C3TA11591G